

---

# Graphical Generative Adversarial Networks

---

Chongxuan Li<sup>1</sup> Max Welling<sup>2</sup> Jun Zhu<sup>1</sup> Bo Zhang<sup>1</sup>

## Abstract

We propose Graphical Generative Adversarial Networks (Graphical-GAN) to model structured data. Graphical-GAN conjoins the power of Bayesian networks on compactly representing the dependency structures among random variables and that of generative adversarial networks on learning expressive dependency functions. We introduce a structured recognition model to infer the posterior distribution of latent variables given observations. We propose two alternative divergence minimization approaches to learn the generative model and recognition model jointly. The first one treats all variables as a whole, while the second one utilizes the structural information by checking the individual local factors defined by the generative model and works better in practice. Finally, we present two important instances of Graphical-GAN, i.e. Gaussian Mixture GAN (GMGAN) and State Space GAN (SSGAN), which can successfully learn the discrete and temporal structures on visual datasets, respectively.

## 1. Introduction

Deep implicit models (Mohamed & Lakshminarayanan, 2016) have shown promise on synthesizing realistic images (Goodfellow et al., 2014; Radford et al., 2015; Arjovsky et al., 2017) and inferring latent variables (Mescheder et al., 2017; Huszár, 2017). However, these approaches do not explicitly model the underlying structures of the data, which are common in practice (e.g., temporal structures in videos). Probabilistic graphical models (Koller & Friedman, 2009) provide principle ways to incorporate the prior knowledge about the data structures but these models often lack the capability to deal with the complex data like images.

To conjoin the benefits of both worlds, we propose a flexible generative modelling framework called Graphical Gen-

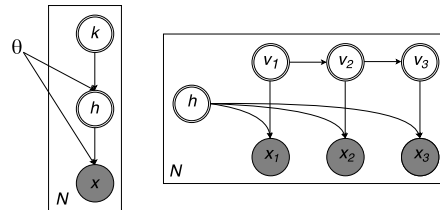


Figure 1. Two instances of Graphical-GAN. Left: GMGAN. Right: SSGAN. The grey and white units represent the observed and latent variables, respectively. The single and double circles represent the deterministic and stochastic variables, respectively. We omit the global parameter  $\theta$  in SSGAN for simplicity.

erative Adversarial Networks (Graphical-GAN). On one hand, Graphical-GAN employs Bayesian networks (Koller & Friedman, 2009) to represent the structures among variables. On the other hand, Graphical-GAN uses deep implicit likelihood functions (Goodfellow et al., 2014) to model complex data. See Fig. 1 for two instances of Graphical-GAN.

Graphical-GAN is sufficiently flexible to model structured data but the inference and learning are challenging due to the presence of deep implicit likelihoods. For inference, we build a structured recognition model to approximate the true posterior distribution. Two families of the recognition models, i.e. the *mean field posteriors* (Jordan et al., 1999) and the *inverse factorizations* (Stuhlmüller et al., 2013) are studied in this paper. For learning, we propose two algorithms based on divergence minimization and both use the adversarial technique (Goodfellow et al., 2014) to estimate the divergence. The first *global* algorithm treats all variables as a whole as in (Dumoulin et al., 2016; Donahue et al., 2016), while the second *local* algorithm discriminates the individual local factors defined by the generative model separately. The local one works better empirically as it utilizes the structural information.

When applied to a specific scenario, the generative model is determined a priori by context or domain knowledge and the proposed approximate inference and learning algorithms are generally applicable to arbitrary Graphical-GAN. As instances, we present Gaussian Mixture GAN (GMGAN) and State Space GAN (SSGAN) to learn the discrete and temporal structures on visual datasets, respectively. Empirically, these models can generate structured samples and learn interpretable features given the data. Further, the learned features

---

<sup>1</sup>Tsinghua University, Beijing, China <sup>2</sup>University of Amsterdam, Amsterdam, Netherlands. Correspondence to: Chongxuan Li <chongxuanli1991@gmail.com>, Jun Zhu <dc-szj@mail.tsinghua.edu.cn>.

can be useful in some applications like clustering and reconstruction, where the performance of Graphical-GAN is at least comparable or superior to the existing models.

Overall, our contributions are as follows:

- We propose Graphical-GAN, a general generative modelling framework for structured data;
- We present two instances of Graphical-GAN to learn the discrete and temporal structures, respectively;
- Empirical results show the promise of Graphical-GAN on generative modelling of structured data.

## 2. General Method

In this section, we present the general framework with model definition, approximate inference and learning algorithms.

### 2.1. Model

We assume that we have  $N$  i.i.d. samples from the joint distribution  $p_{\mathcal{G}}(X, Z) = p_{\mathcal{G}}(Z)p_{\mathcal{G}}(X|Z)$ , where  $\mathcal{G}$  is the associated directed acyclic graph (DAG), and  $X$  and  $Z$  denote the observable variables and latent variables, respectively. According to the local structures of  $\mathcal{G}$ , the distribution of a single data point can be further factorized as follows:

$$p_{\mathcal{G}}(X, Z) = \prod_{i=1}^{|Z|} p(z_i | \text{pa}_{\mathcal{G}}(z_i)) \prod_{j=1}^{|X|} p(x_j | \text{pa}_{\mathcal{G}}(x_j)), \quad (1)$$

where  $\text{pa}_{\mathcal{G}}(x)$  denotes the parents of  $x$  in the associated graph  $\mathcal{G}$ . Note that  $\text{pa}_{\mathcal{G}}(x)$  may contain both latent and observable variables. Following the factorization, we can sample from the model efficiently via *ancestral sampling*.

Given the dependency structures, the dependency functions among the variables can be parameterized as deep neural networks to fit complicated data. As for the likelihood functions, we consider *implicit probabilistic models* (Mohamed & Lakshminarayanan, 2016) instead of *prescribed probabilistic models*. Prescribed models (Kingma & Welling, 2013) define the likelihood functions for  $X$  with an explicit specification. In contrast, implicit models (Goodfellow et al., 2014) deterministically transform  $Z$  to  $X$  and the likelihood can be intractable. We focus on implicit models because they have been proven effective on image generation (Radford et al., 2015; Arjovsky et al., 2017) and the learning algorithms for implicit models can be easily extended to prescribed models. We also directly compare with existing structured prescribed models (Dilokthanakul et al., 2016) in Sec. 5.2. Following the well established literature, we refer to our model as Graphical Generative Adversarial Networks (Graphical-GAN).

The inference and learning of Graphical-GAN are nontrivial. On one hand, Graphical-GAN employs highly nonlinear

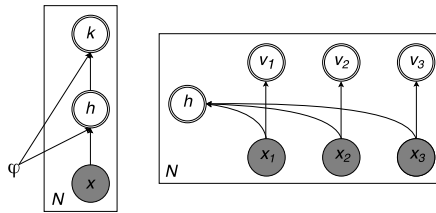


Figure 2. Recognition models. Left: the inverse factorization on GMGAN. Right: the mean-field posterior on SSGAN.

and hence not invertible neural networks, which makes the posterior distribution of the latent variables intractable. On the other hand, the model is defined without a proper likelihood function on the data, which makes the likelihood based learning methods infeasible. We address these problems via amortized inference and divergence minimization approaches, as detailed in Sec. 2.2 and Sec. 2.3, respectively.

### 2.2. Approximate Inference

We leverage recent advances on *amortized inference* of deep generative models (Kingma & Welling, 2013; Dumoulin et al., 2016; Donahue et al., 2016; Tolstikhin et al., 2017) to infer the latent variables given the data. Basically, these approaches introduce a recognition model, which is a family of distributions of a simple form, to approximate the true posterior. The recognition model is shared by all data points and often parameterized as a deep neural network.

The problem is more complicated in our case because we need to further consider the structures during the inference procedure. Naturally, we introduce a structured recognition model with an associated graph  $\mathcal{H}$  as the approximate posterior, which is formally given by:

$$q_{\mathcal{H}}(Z|X) = \prod_{i=1}^{|Z|} q(z_i | \text{pa}_{\mathcal{H}}(z_i)). \quad (2)$$

Given data points from the true data distribution  $q(X)$ , we can obtain samples following the joint distribution  $q_{\mathcal{H}}(X, Z) = q(X)q_{\mathcal{H}}(Z|X)$  efficiently via ancestral sampling. Considering different dependencies among the variables, or equivalently  $\mathcal{H}$ s, we study two types of recognition models: the mean-field posteriors (Jordan et al., 1999) and the inverse factorizations (Stuhlmüller et al., 2013).

The mean-field assumption has been widely adopted to variational inference methods (Jordan et al., 1999) because of its simplicity. In such methods, all of the dependency structures among the latent variables are ignored and the approximate posterior could be factorized as follows:

$$q_{\mathcal{H}}(Z|X) = \prod_{i=1}^{|Z|} q(z_i | X), \quad (3)$$

where the associated graph  $\mathcal{H}$  has fully factorized structures.

---

**Algorithm 1** The global algorithm for Graphical-GAN
 

---

**repeat**

- Get a minibatch of samples from  $p(X, Z)$
- Get a minibatch of samples from  $q(X, Z)$
- Estimate the divergence  $\mathcal{D}(q(X, Z)||p(X, Z))$  using Eqn. (6) and the current value of  $\psi$
- Update  $\psi$  to maximize the divergence
- Get a minibatch of samples from  $p(X, Z)$
- Get a minibatch of samples from  $q(X, Z)$
- Estimate the divergence  $\mathcal{D}(q(X, Z)||p(X, Z))$  using Eqn. (6) and the current value of  $\psi$
- Update  $\theta$  and  $\phi$  to minimize the divergence

**until** Convergence or reaching certain threshold
 

---



---

**Algorithm 2** The local algorithm for Graphical-GAN
 

---

**repeat**

- Get a minibatch of samples from  $p(X, Z)$
- Get a minibatch of samples from  $q(X, Z)$
- Approximate the divergence  $\mathcal{D}(q(X, Z)||p(X, Z))$  using Eqn. (12) and the current value of  $\psi$
- Update  $\psi$  to maximize the divergence
- Get a minibatch of samples from  $p(X, Z)$
- Get a minibatch of samples from  $q(X, Z)$
- Approximate the divergence  $\mathcal{D}(q(X, Z)||p(X, Z))$  using Eqn. (12) and the current value of  $\psi$
- Update  $\theta$  and  $\phi$  to minimize the divergence

**until** Convergence or reaching certain threshold
 

---

The inverse factorizations (Stuhlmüller et al., 2013) approach views the original graphical model as a *forward factorization* and samples the latent variables given the observations efficiently by inverting  $\mathcal{G}$  step by step. Formally, the *inverse factorization* is defined as follows:

$$q_{\mathcal{H}}(Z|X) = \prod_{i=1}^{|Z|} q(z_i | \partial_{\mathcal{G}}(z_i) \cap z_{>i}), \quad (4)$$

where  $\partial_{\mathcal{G}}(z_i)$  denotes the *Markov blanket* of  $z_i$  on  $\mathcal{G}$  and  $z_{>i}$  denotes all  $z$  after  $z_i$  in a certain order, which is defined from leaves to roots according to the structure of  $\mathcal{G}$ . See the formal algorithm to build  $\mathcal{H}$  based on  $\mathcal{G}$  in Appendix A.

Given the structures of the approximate posteriors, we also parameterize the dependency functions as neural networks of similar sizes to those in the generative models. Both posterior families are generally applicable for arbitrary Graphical-GAN and we use them in two different instances, respectively. See Fig. 2 for an illustration.

### 2.3. Learning Algorithms

Now, our goal is to learn the parameters in the generative model and the recognition model jointly. We present two algorithms based on divergence minimization.

#### 2.3.1. THE GLOBAL ALGORITHM

The first *global* algorithm ignores the structural information and directly minimizes certain divergence between  $p(X, Z)$  and  $q(X, Z)$ . Let  $\theta$  and  $\phi$  denote the parameters in the generative model and the recognition model, respectively. Formally, the learning problem is given by:

$$\min_{\theta, \phi} \mathcal{D}(q(X, Z)||p(X, Z)), \quad (5)$$

where we omit the subscripts of the associated graphs for simplicity. We restrict  $\mathcal{D}$  in the  $f$ -divergence family (Csiszár et al., 2004), that is  $\mathcal{D}(q(X, Z)||p(X, Z)) =$

$\int p(X, Z) f\left(\frac{q(X, Z)}{p(X, Z)}\right) dX dZ$ , where  $f$  is a convex function of the likelihood ratio. The Kullback-Leibler (KL) divergence and the Jensen-Shannon (JS) divergence are included.

The learning problem (5) cannot be optimized directly because the likelihood ratio is unknown given the implicit  $p(X, Z)$ . One solution is to use a parametric discriminator to estimate the divergence  $\mathcal{D}(q(X, Z)||p(X, Z))$  based on only samples (Goodfellow et al., 2014). ALI (Dumoulin et al., 2016; Donahue et al., 2016) is a special case of this approach by minimizing the JS divergence, i.e.  $\mathcal{D}_{JS}$ . Formally, the estimate of the divergence is given by:

$$\max_{\psi} \mathbb{E}_q[\log(D(X, Z))] + \mathbb{E}_p[\log(1 - D(X, Z))], \quad (6)$$

where  $D$  is the discriminator introduced for divergence estimation and  $\psi$  denotes the parameters in  $D$ . If  $D$  is Bayes optimal, then the estimate actually equals to  $2\mathcal{D}_{JS}(q(X, Z)||p(X, Z)) - \log 4$  (Dumoulin et al., 2016; Donahue et al., 2016), which is equivalent to  $\mathcal{D}_{JS}(q(X, Z)||p(X, Z))$ . Using the solution provided by the  $f$ -GAN (Nowozin et al., 2016), we can optimize the general  $f$ -divergence, which slightly extends ALI.

We can directly adopt this approach to our Graphical-GAN (See Alg. 1) and it is theoretically sound under the non-parametric assumptions (Donahue et al., 2016; Dumoulin et al., 2016). However, it may fail in practice because the capability of a single discriminator is insufficient given data with complicated structures, which makes the estimate of the divergence not reliable. Intuitively, the problem will be easier if we also consider the data structures when discriminating the samples. The intuition motivates us to propose the second local learning algorithm, shown as follows.

#### 2.3.2. THE LOCAL ALGORITHM

We follow the recipe of the generic message passing procedure (Minka, 2005) to obtain the *local* algorithm, which tries to match the local factors of  $p(X, Z)$  and  $q(X, Z)$ . We start from the factorization of  $p(X, Z)$  in terms of a set of

factors  $F_G$ , which is given by:

$$p(X, Z) \propto \prod_{A \in F_G} p(A). \quad (7)$$

Generally, we can choose any reasonable  $F_G^1$  but here we specify that  $F_G$  consists of  $(x, \text{pa}_G(x))$  and  $(z, \text{pa}_G(z))$  for all  $x$  and  $z$  in the model.

We first assume that the recognition model can also be factorized in the same way. Namely, we have

$$q(X, Z) \propto \prod_{A \in F_G} q(A). \quad (8)$$

Then we're going to minimize the divergence in terms of each factor individually. For factor  $A$ , we're interested in optimizing the following local divergence (Minka, 2005):

$$\mathcal{D}(q(A)\overline{q(\bar{A})}||p(A)\overline{p(\bar{A})}), \quad (9)$$

where  $\overline{p(\bar{A})}$  denotes the marginal distribution over the complementary  $\bar{A}$  of  $A$ . In traditional message passing (Minka, 2005), it is commonly assumed that  $q(\bar{A}) \approx \overline{p(\bar{A})}$  to make the expression tractable. Though the approximation cannot be justified theoretically, some intuition and empirical results (Minka, 2005) suggest that the gap is small if the approximate posterior is a good fit to the true posterior. Given the approximation, for factor  $A$ , the objective changes to:

$$\mathcal{D}(q(A)\overline{q(\bar{A})}||p(A)\overline{q(\bar{A})}). \quad (10)$$

In our approach, we make the same assumption because  $\overline{q(\bar{A})}$  will be cancelled in the likelihood ratio if  $\mathcal{D}$  belongs to  $f$ -divergence and we can ignore other factors when discriminating  $q(A)$ , which reduces the complexity of the problem. For instance, we can approximate the JS divergence for every factor  $A$  as:

$$\mathcal{D}_{JS}(q(X, Z)||p(X, Z)) \approx \mathbb{E}_q[\log \frac{q(A)}{m(A)}] + \mathbb{E}_p[\log \frac{p(A)}{m(A)}],$$

where  $m(A) = \frac{1}{2}(p(A) + q(A))$ . See Appendix B for the derivation. As we are doing amortized inference, we further average the divergences over all local factors as:

$$\begin{aligned} & \frac{1}{|F_G|} \sum_{A \in F_G} \left[ \mathbb{E}_q[\log \frac{q(A)}{m(A)}] + \mathbb{E}_p[\log \frac{p(A)}{m(A)}] \right] = \\ & \frac{1}{|F_G|} \left[ \mathbb{E}_q[\sum_{A \in F_G} \log \frac{q(A)}{m(A)}] + \mathbb{E}_p[\sum_{A \in F_G} \log \frac{p(A)}{m(A)}] \right]. \quad (11) \end{aligned}$$

The equality holds due to the linearity of the expectation. The expression in Eqn. (11) provides an efficient solution

<sup>1</sup>For instance, the global algorithm is a special case where  $F_G$  has only one factor that involves all variables.

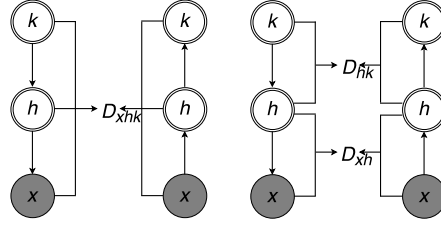


Figure 3. Left: the global algorithm. Right: the local algorithm.

where we can obtain samples over the entire variable space once and repeatedly project the samples into each factor. Finally, we can estimate all local divergences using individual discriminators and the objective function is as follows:

$$\begin{aligned} & \max_{\psi} \frac{1}{|F_G|} \mathbb{E}_q[\sum_{A \in F_G} \log(D_A(A))] \\ & + \frac{1}{|F_G|} \mathbb{E}_p[\sum_{A \in F_G} \log(1 - D_A(A))], \quad (12) \end{aligned}$$

where  $D_A$  denotes the discriminator for the factor  $A$  and  $\psi$  denotes the parameters in all discriminators.

Though we assume that  $q(X, Z)$  shares the same factorization with  $p(X, Z)$  as in Eqn. (8) when deriving the objective function, the result in Eqn. (12) does not specify the form of  $q(X, Z)$ . This is because we do not need to compute  $q(A)$  explicitly and instead we directly estimate the likelihood ratio based on samples. This makes it possible for Graphical-GAN to use an arbitrary  $q(X, Z)$ , including the mean-field posteriors and inverse factorizations proposed in Sec. 2.2, as long as we can sample from it quickly.

We summarize the procedure in Alg. 2 and illustrate both algorithms on GMGAN in Fig. 3 for a clearer comparison. Our local algorithm is closely related to the work of (Karaletsos, 2016), in which a factor of  $p$  and the corresponding factor of  $q$  may consist of different variables in general and hence cannot be discriminated via a typical network in practice. See Sec. 4 for a detailed comparison.

Given the divergence estimate, we perform the stochastic gradient decent to update the parameters. We use the reparameterization trick (Kingma & Welling, 2013) and the Gumbel-Softmax trick (Jang et al., 2016) to estimate the gradients with continuous and discrete random variables, respectively. See (Schulman et al., 2015) for a systematical study of estimating gradients in stochastic graphs.

### 3. Two Instances

We consider two common and typical scenarios involving structured data in practice. In the first one, the dataset consists of images with discrete attributes or classes but the groundtruth for an individual sample is unknown. In the second one, the dataset consists of sequences of im-

ages with temporal dependency within each sequence. In both cases, we would like to generate meaningful samples by controlling the latent variables and learn interpretable representations given the data. We present two important instances of Graphical-GAN, i.e. Gaussian Mixture GAN (GMGAN) and State Space GAN (SSGAN), to deal with these two scenarios, respectively. These instances show the abilities of our general framework to deal with discrete latent variables and complex structures, respectively.

### 3.1. GMGAN

GMGAN assumes that the data consists of  $K$  mixtures and hence uses a mixture of Gaussian prior. Formally, the generative process of GMGAN is:

$$k \sim \text{Cat}(\pi), h|k \sim \mathcal{N}(\mu_k, \Sigma_k), x|h = G(h),$$

where  $Z = (k, h)$ , and  $\pi$  and  $G$  are the coefficient vector and the generator, respectively. We assume that  $\pi$  and  $\Sigma_k$ s are fixed as the uniform prior and identity matrices, respectively. Namely, we only have a few extra trainable parameters, i.e. the means for the mixtures  $\mu_k$ s.

We use the inverse factorization as the recognition model because it preserves the dependency relationships in the model. The resulting approximate posterior is a simple inverse chain as follows:

$$h|x = E(x), q(k|h) = \frac{\pi_k \mathcal{N}(h|\mu_k, \Sigma_k)}{\sum_{k'} \pi_{k'} \mathcal{N}(h|\mu_{k'}, \Sigma_{k'})},$$

where  $E$  is the extractor that maps data points to the latent variables.

In the global algorithm, a single network is used to discriminate the  $(x, h, k)$  tuples. In the local algorithm, two separate networks are introduced to discriminate the  $(x, h)$  and  $(h, k)$  pairs, respectively. See Fig. 3 for an illustration.

### 3.2. SSGAN

SSGAN assumes that there are two types of latent variables. One is invariant across the time, denoted as  $h$  and the other varies across the time, denoted as  $v_t$  for time stamp  $t = 1, \dots, T$ . Further, SSGAN assumes that  $v_t$ s form a Markov Chain. Formally, the generative process of SSGAN is:

$$\begin{aligned} v_1 &\sim \mathcal{N}(0, I), h \sim \mathcal{N}(0, I), \\ \epsilon_t &\sim \mathcal{N}(0, I), \forall t = 1, 2, \dots, T-1, \\ v_{t+1}|v_t &= O(v_t, \epsilon_t), \forall t = 1, 2, \dots, T-1, \\ x_t|h, v_t &= G(h, v_t), \forall t = 1, 2, \dots, T, \end{aligned}$$

where  $Z = (h, v_1, \dots, v_T)$ , and  $O$  and  $G$  are the transition operator and the generator, respectively. Note that  $O$  and  $G$  are shared across the time under the stationary and output independent assumptions, respectively.

For simplicity, we use the mean-field recognition model as the approximate posterior, which is given by:

$$\begin{aligned} h|x_1, x_2, \dots, x_T &= E_1(x_1, x_2, \dots, x_T), \\ v_t|x_1, x_2, \dots, x_T &= E_2(x_t), \forall t = 1, 2, \dots, T, \end{aligned}$$

where  $E_1$  and  $E_2$  are the extractors that map the data points to  $h$  and  $v$  respectively.  $E_2$  is also shared across the time.

In the global algorithm, a single network is used to discriminate the  $(x_1, \dots, x_T, v_1, \dots, v_T, h)$  samples. In the local algorithm, two separate networks are introduced to discriminate the  $(v_t, v_{t+1})$  pairs and  $(x_t, v_t, h)$  tuples, respectively. Both networks are shared across the time, as well.

## 4. Related Work

**General framework** The work of (Johnson et al., 2016) and (Karaletsos, 2016) are two closest papers on the structured deep generative models. Johnson et al. (2016) introduce structured Bayesian priors to Variational Auto-Encoders (VAE) (Kingma & Welling, 2013) and propose efficient inference algorithms with conjugated exponential family structure. Compared to (Johnson et al., 2016), Graphical-GAN is more flexible on the model definition and learning methods, and hence can deal with natural data.

Adversarial Message Passing (AMP) (Karaletsos, 2016) also considers structured implicit models. A key difference is that, for every  $i$ , AMP discriminates  $(z_i, \text{pa}_{\mathcal{H}}(z_i))$  of  $q$  and  $(z_{i+1}, \text{pa}_{\mathcal{G}}(z_{i+1}))$  of  $p$ . Note that the factor pairs may consist of different variables and have different dimensionalities in general. Therefore, AMP is not practical because a typical discriminator cannot take two types of inputs with different dimensionalities. Further, no empirical evidence is reported in (Karaletsos, 2016). In contrast, Graphical-GAN has no restriction on the form of  $q$  by considering only  $(z_i, \text{pa}_{\mathcal{G}}(z_i))$  and achieves excellent empirical results (See Sec. 5).

There is much work on the learning and inference of implicit models.  $f$ -GAN (Nowozin et al., 2016) and WGAN (Arjovsky et al., 2017) generalize the original GAN using the  $f$ -divergence and Wasserstein distance, respectively. ALI (Donahue et al., 2016; Dumoulin et al., 2016) introduces an inference network to GAN for representation learning. The recent work of (Tolstikhin et al., 2017) minimizes a penalized form of the Wasserstein distance in the optimal transport point of view and naturally considers both the generative modelling and inference together. The Wasserstein distance can also be used in Graphical-GAN to generalize our current algorithms and we leave it for the future work.

**Instances** Several methods have learned the discrete structures in an unsupervised manner. Makhzani et al. (2015) extend an autoencoder to a generative model by matching the *aggregated posterior* to a prior distribution and shows the ability to cluster handwritten digits. (Chen et al., 2016) in-

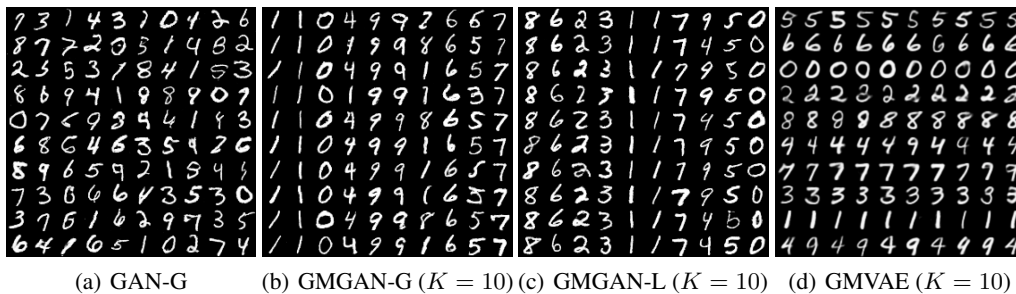


Figure 4. Samples on the MNIST dataset. The results of (a) are comparable to those reported in (Donahue et al., 2016). The mixture  $k$  is fixed in each column of (b) and (c). The mixture  $k$  is fixed in each row of (d). The results of (d) are from (Dilokthanakul et al., 2016).

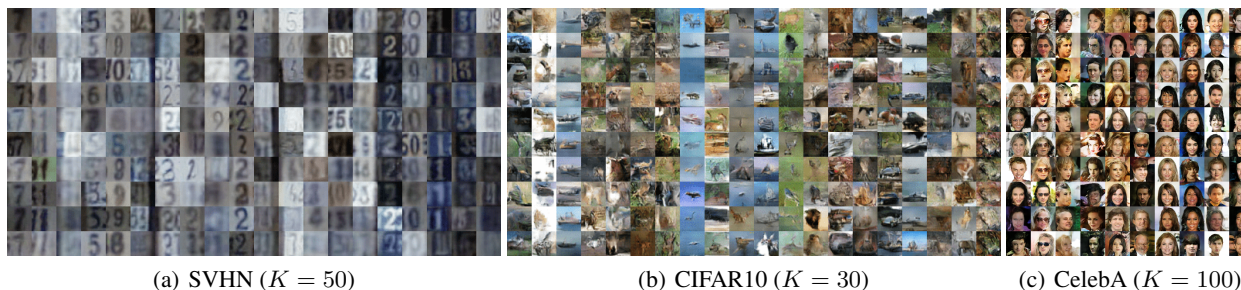


Figure 5. Part of samples of GMGAN-L on three datasets. The mixture  $k$  is fixed in each column. See the complete results in Appendix D.

produce some interpretable codes independently from other latent variables and the model is learned via regularizing the original GAN loss with the mutual information between the codes and the data. In contrast, GMGAN explicitly builds a hierarchical model with top-level discrete codes and no regularization is required. The most direct competitor (Dilokthanakul et al., 2016) extends VAE (Kingma & Welling, 2013) with a mixture of Gaussian prior and is compared with GMGAN in Sec. 5.2.

There exist extensive prior methods on synthesizing videos but most of them condition on input frames (Srivastava et al., 2015; Oh et al., 2015; Mathieu et al., 2015; Kalchbrenner et al., 2016; Xue et al., 2016; Villegas et al., 2017; Denton & Birodkar, 2017). To our best knowledge, only two existing methods (Vondrick et al., 2016; Saito & Matsumoto, 2016) can generate videos without input frames. In both methods, all latent variables are generated together without structures. In contrast, SSGAN explicitly disentangles the invariant latent variables from the variant ones and builds a Markov chain on the variant ones, which make it possible to learn interpretable features and generalize to longer sequences.

## 5. Experiments

In our experiments, we are going to show that

- Graphical-GAN can generate structured samples and learn interpretable features given the data;
- The learned features can be useful in applications such as clustering and the performance of Graphical-GAN

is comparable or superior to existing methods;

- The local algorithm outperforms the global algorithm, especially when the structure is complex.

### 5.1. Experimental settings

We implement our model using the TensorFlow (Abadi et al., 2016) library.<sup>2</sup> In all experiments, we optimize the JS-divergence. We use the widely adopted DCGAN architecture (Radford et al., 2015) in all experiments to fairly compare Graphical-GAN with existing methods. The model size and the usage of the batch normalization (Ioffe & Szegedy, 2015) depend on the data. The size of  $h$  in both GMGAN and SSGAN is 128 and the size of  $v$  in SSGAN is 8. All models are trained with the ADAM optimizer (Kingma & Ba, 2014) with  $\beta_1 = 0.5$  and  $\beta_2 = 0.999$ . The learning rate is fixed as 0.0002 in GMGAN and 0.0001 in SSGAN. See Appendix C and our source code for further details.

### 5.2. GMGAN Learns Discrete Structures

We evaluate GMGAN on the MNIST (Schölkopf & Smola, 2002), SVHN (Netzer et al., 2011), CIFAR10 (Krizhevsky & Hinton, 2009) and CelebA (Liu et al., 2015) datasets. The MNIST dataset consists of handwritten digits of size  $28 \times 28$  and there are 50,000 training samples, 10,000 validation samples and 10,000 testing samples. The SVHN dataset consists of digit sequences of size  $32 \times 32$ , and there are 73,257 training samples and 26,032 testing samples. The

<sup>2</sup>Our source code will be available at <https://github.com/zhenxuan00/graphical-gan>.

Table 1. Unsupervised clustering accuracies on the MNIST dataset. Baseline results are from (Dilokthanakul et al., 2016) and our results are averaged over 10 runs with different random seeds.

ALGORITHM	$K$	ACCURACY
<i>GMVAE</i>	30	92.77 ( $\pm 1.60$ )
<i>GMGAN-G</i> (OURS)	30	91.62 ( $\pm 1.91$ )
<i>GMGAN-L</i> (OURS)	30	93.03 ( $\pm 1.65$ )
<i>CatGAN</i>	20	90.30
<i>AAE</i>	16	90.45 ( $\pm 2.05$ )
<i>AAE</i>	30	95.90 ( $\pm 1.13$ )



(a) GAN-G (b) GMGAN-L (c) GAN-G (d) GMGAN-L

Figure 6. Reconstruction on the MNIST and SVHN datasets. Each odd column shows the test inputs and the next even column shows the corresponding reconstruction. (a) and (c) are comparable to those reported in (Donahue et al., 2016; Dumoulin et al., 2016).

CIFAR10 dataset consists of natural images of size  $32 \times 32$  and there are 50,000 training samples and 10,000 testing samples. The CelebA dataset consists of 202,599 faces and we randomly sample 5,000 samples for testing. Further, the faces are center cropped and downsampled to size  $64 \times 64$ . We focus on the unsupervised learning setting here. Our assumption is that there exist discrete structures, e.g. classes and attributes, in the data but the ground truth is unknown.

We compare Graphical-GAN with two existing baselines, i.e. ALI (Donahue et al., 2016; Dumoulin et al., 2016) and GMVAE (Srivastava et al., 2015). For simplicity, we denote GMGAN trained with the global and local algorithms as *GMGAN-G* and *GMGAN-L*, respectively. Following this, we also denote ALI as *GAN-G*.

We first compare the samples generated by all models on the MNIST dataset, as shown in Fig. 4. The samples of GMGAN-G and GMGAN-L are at least comparable to those of GAN-G (i.e. ALI), and are sharper than those of the GMVAE. Besides, the clustering performance of GMGAN-L is superior to GMGAN-G and GMVAE with less ambiguous clusters. We also present the quantitative results in Tab. 1 following (Dilokthanakul et al., 2016). After clustering the test samples, we first find the sample that is nearest to the centroid of each cluster and use the label of that sample as the prediction of the testing samples in the same cluster. Again, GMGAN-L outperforms GMGAN-G and GMVAE.

We then demonstrate the ability of GMGAN-L to deal with more challenging datasets. The samples on the SVHN, CIFAR10 and CelebA datasets are shown in Fig. 5. Given a

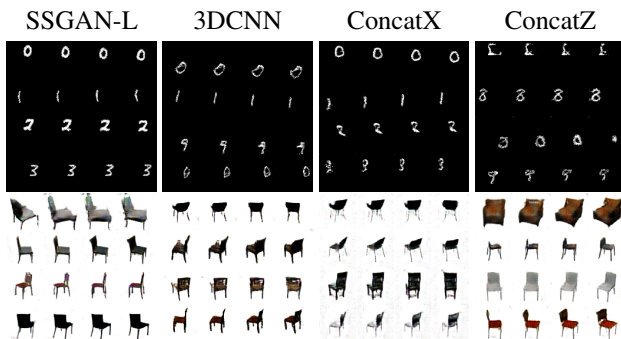


Figure 7. Samples on the Moving MNIST and 3D chairs datasets when  $T = 4$ . Each row in a subfigure represents a video sample.

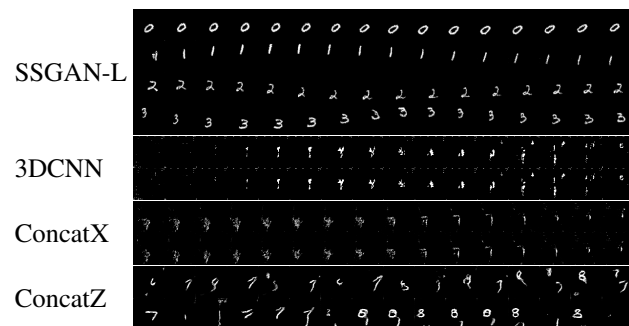


Figure 8. Samples on the Moving MNIST dataset when  $T = 16$ .

fixed mixture  $k$ , GMGAN-L can generate samples with similar semantics and visual factors, including the object classes, backgrounds and attributes like “wearing glasses”. Besides, the sample quality is better than the existing methods with similar architectures. In our implementation, GMGAN-L achieves the inception score of  $5.94 (\pm 0.06)$  while GAN-G only achieves  $5.26 (\pm 0.05)$ , which is consistent with  $5.34 (\pm 0.05)$  reported in (Warde-Farley & Bengio, 2016).

We further present the reconstruction results in Fig. 6. GMGAN-L outperforms GAN-G significantly in terms of preserving the same semantics and similar visual appearance. Besides, GMGAN-L achieves the mean square error (MSE) of  $0.044 (\pm 0.001)$  while GAN-G only achieves  $0.071 (\pm 0.001)$  on the MNIST dataset. Intuitively, this is because the Gaussian mixture prior helps the model learn a more spread latent space with less ambiguous areas shared by samples in different classes.

Finally, we show the samples of GMGAN-L by varying  $K$  and linearly interpolating the latent variables in Appendix D.

### 5.3. SSGAN Learns Temporal Structures

We evaluate SSGAN on the Moving MNIST (Srivastava et al., 2015) and 3D chairs (Aubry et al., 2014) datasets. In the Moving MNIST dataset, each clip contains a handwritten digit which bounces inside a  $64 \times 64$  patch. The velocity of the digit is randomly sampled and fixed within a clip. We generate two datasets of length 4 and length 16, respectively.

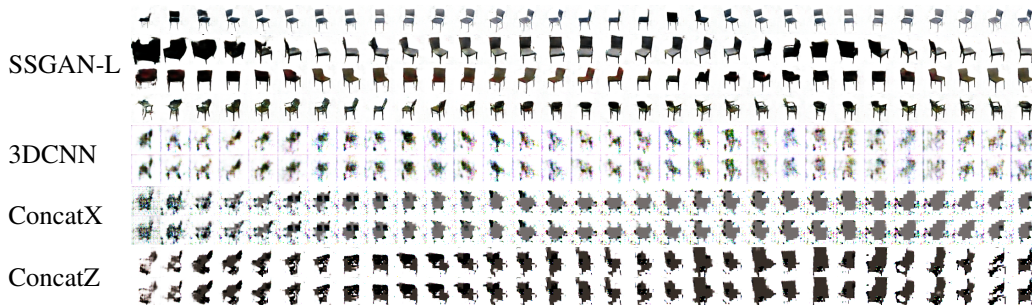


Figure 9. Samples on the 3D chairs dataset when  $T = 31$ .



Figure 10. Disentanglement results when  $T = 16$ . Each odd row shows a video in the testing set and the next even row shows the video generated with a fixed invariant feature  $h$  and the dynamic features  $v$  inferred from the corresponding test video.

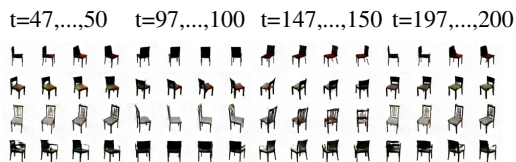


Figure 11. 16 of 200 frames generated by SSGAN-L in each row.

To improve the sample quality, all models condition on the label information as in (Radford et al., 2015). The 3D chairs dataset consists of 2,786 sequences of rendered chairs and each sequence is of length 31. We randomly sample subsequences if necessary. The clips in the 3D chairs dataset are center cropped and downsampled to size  $64 \times 64$ . No supervision is used on the 3D chairs dataset.

We denote the SSGAN model trained with the local algorithm as *SSGAN-L*. We construct three types of baseline models, which are trained with our global learning algorithm but use discriminators with different architectures. The *ConcatX* baseline concatenates all input frames together and processes the input as a whole image with a typical convolutional neural network (CNN). The *ConcatZ* baseline processes the input frames independently using a typical CNN and concatenates the features as the input for fully connected layers to obtain the latent variables. The *3DCNN* baseline uses a 3D CNN to process the whole input directly. In particular, the 3DCNN baseline is quite similar to the existing generative models (Vondrick et al., 2016; Saito & Matsumoto, 2016). The key difference is that we omit the two stream architecture proposed in (Vondrick et al., 2016) and the singular value clipping proposed in (Saito & Matsumoto, 2016) for fair comparison. Also note that our

contribution is orthogonal to these techniques.

If  $T = 4$ , then all models can generate reasonable samples on both datasets, as shown in Fig. 7. However, if the structure of the data gets complicated, i.e.  $T = 16$  on Moving MNIST and  $T = 31$  on 3D chairs, all baseline models fail while SSGAN-L can still successfully track the movement of the object and approximately preserve the visual appearance, as shown in Fig. 8 and Fig. 9, respectively. Intuitively, this is because the nonparametric assumption is too strong and a single discriminator cannot provide reliable divergence estimate with limited capability in practise. See the reconstruction results of SSGAN-L in Appendix E.

Compared with existing GAN models (Vondrick et al., 2016; Saito & Matsumoto, 2016) on videos, SSGAN-L can learn interpretable features by explicitly considering the structures. We present the disentanglement results on the 3D chairs dataset in Fig. 10. On one hand, the samples share the same semantics given by a fixed  $h$ . On the other hand, the samples can track the temporal dynamics using the  $v$  inferred from the corresponding test video. Existing methods (Villegas et al., 2017; Denton & Birodkar, 2017) on learning interpretable features from videos rely on regularization terms to ensure the disentanglement while SSGAN uses pure adversarial losses.

Finally, we show the generalization ability of SSGAN in Fig. 11. Though trained on videos of length 31, SSGAN can generate much longer sequences, which again demonstrates the advantages of SSGAN over existing generative models (Vondrick et al., 2016; Saito & Matsumoto, 2016).

## 6. Conclusion

This paper introduces a flexible generative modelling framework called Graphical Generative Adversarial Networks (Graphical-GAN). Graphical-GAN provides a general solution to utilize the underlying structural information of the data. Empirical results of two instances show the promise of Graphical-GAN on learning interpretable representations and generating structured samples. Possible extensions to Graphical-GAN include: generalized learning and inference algorithms, instances with more complicated structures (e.g.,



trees) and semi-supervised learning for structured data.

## References

- Abadi, Martín, Barham, Paul, Chen, Jianmin, Chen, Zhifeng, Davis, Andy, Dean, Jeffrey, Devin, Matthieu, Ghemawat, Sanjay, Irving, Geoffrey, Isard, Michael, et al. TensorFlow: A system for large-scale machine learning. 2016.
- Arjovsky, Martin, Chintala, Soumith, and Bottou, Léon. Wasserstein GAN. *arXiv preprint arXiv:1701.07875*, 2017.
- Aubry, Mathieu, Maturana, Daniel, Efros, Alexei A, Russell, Bryan C, and Sivic, Josef. Seeing 3D chairs: exemplar part-based 2D-3D alignment using a large dataset of cad models. In *Proceedings of the IEEE conference on computer vision and pattern recognition*, pp. 3762–3769, 2014.
- Chen, Xi, Duan, Yan, Houthoofd, Rein, Schulman, John, Sutskever, Ilya, and Abbeel, Pieter. InfoGAN: Interpretable representation learning by information maximizing generative adversarial nets. In *Advances in Neural Information Processing Systems*, pp. 2172–2180, 2016.
- Csiszár, Imre, Shields, Paul C, et al. Information theory and statistics: A tutorial. *Foundations and Trends® in Communications and Information Theory*, 1(4):417–528, 2004.
- Denton, Emily and Birodkar, Vighnesh. Unsupervised learning of disentangled representations from video. In *Advances in Neural Information Processing Systems*, pp. 4417–4426, 2017.
- Dilokthanakul, Nat, Mediano, Pedro AM, Garnelo, Marta, Lee, Matthew CH, Salimbeni, Hugh, Arulkumaran, Kai, and Shanahan, Murray. Deep unsupervised clustering with Gaussian mixture variational autoencoders. *arXiv preprint arXiv:1611.02648*, 2016.
- Donahue, Jeff, Krähenbühl, Philipp, and Darrell, Trevor. Adversarial feature learning. *arXiv preprint arXiv:1605.09782*, 2016.
- Dumoulin, Vincent, Belghazi, Ishmael, Poole, Ben, Lamb, Alex, Arjovsky, Martin, Mastropietro, Olivier, and Courville, Aaron. Adversarially learned inference. *arXiv preprint arXiv:1606.00704*, 2016.
- Goodfellow, Ian, Pouget-Abadie, Jean, Mirza, Mehdi, Xu, Bing, Warde-Farley, David, Ozair, Sherjil, Courville, Aaron, and Bengio, Yoshua. Generative adversarial nets. In *Advances in neural information processing systems*, pp. 2672–2680, 2014.
- Huszár, Ferenc. Variational inference using implicit distributions. *arXiv preprint arXiv:1702.08235*, 2017.
- Ioffe, Sergey and Szegedy, Christian. Batch normalization: Accelerating deep network training by reducing internal covariate shift. In *International Conference on Machine Learning*, pp. 448–456, 2015.
- Jang, Eric, Gu, Shixiang, and Poole, Ben. Categorical reparameterization with gumbel-softmax. *arXiv preprint arXiv:1611.01144*, 2016.
- Johnson, Matthew, Duvenaud, David K, Wiltschko, Alex, Adams, Ryan P, and Datta, Sandeep R. Composing graphical models with neural networks for structured representations and fast inference. In *Advances in neural information processing systems*, pp. 2946–2954, 2016.
- Jordan, Michael I, Ghahramani, Zoubin, Jaakkola, Tommi S, and Saul, Lawrence K. An introduction to variational methods for graphical models. *Machine learning*, 37(2): 183–233, 1999.
- Kalchbrenner, Nal, Oord, Aaron van den, Simonyan, Karen, Danihelka, Ivo, Vinyals, Oriol, Graves, Alex, and Kavukcuoglu, Koray. Video pixel networks. *arXiv preprint arXiv:1610.00527*, 2016.
- Karaletsos, Theofanis. Adversarial message passing for graphical models. *arXiv preprint arXiv:1612.05048*, 2016.
- Kingma, Diederik and Ba, Jimmy. Adam: A method for stochastic optimization. *arXiv preprint arXiv:1412.6980*, 2014.
- Kingma, Diederik and Welling, Max. Auto-encoding variational Bayes. *arXiv preprint arXiv:1312.6114*, 2013.
- Koller, Daphne and Friedman, Nir. *Probabilistic graphical models: principles and techniques*. MIT press, 2009.
- Krizhevsky, Alex and Hinton, Geoffrey. Learning multiple layers of features from tiny images. *Technical report, University of Toronto*, 2009.
- Liu, Ziwei, Luo, Ping, Wang, Xiaogang, and Tang, Xiaoou. Deep learning face attributes in the wild. In *Proceedings of International Conference on Computer Vision (ICCV)*, 2015.
- Makhzani, Alireza, Shlens, Jonathon, Jaitly, Navdeep, Goodfellow, Ian, and Frey, Brendan. Adversarial autoencoders. *arXiv preprint arXiv:1511.05644*, 2015.
- Mathieu, Michael, Couprie, Camille, and LeCun, Yann. Deep multi-scale video prediction beyond mean square error. *arXiv preprint arXiv:1511.05440*, 2015.

- Mescheder, Lars, Nowozin, Sebastian, and Geiger, Andreas. Adversarial variational Bayes: Unifying variational autoencoders and generative adversarial networks. *arXiv preprint arXiv:1701.04722*, 2017.
- Minka, Tom. Divergence measures and message passing. Technical report, Microsoft Research, 2005.
- Mohamed, Shakir and Lakshminarayanan, Balaji. Learning in implicit generative models. *arXiv preprint arXiv:1610.03483*, 2016.
- Netzer, Yuval, Wang, Tao, Coates, Adam, Bissacco, Alessandro, Wu, Bo, and Ng, Andrew Y. Reading digits in natural images with unsupervised feature learning. In *NIPS Workshop on Deep Learning and Unsupervised Feature Learning*, 2011.
- Nowozin, Sebastian, Cseke, Botond, and Tomioka, Ryota. f-GAN: Training generative neural samplers using variational divergence minimization. In *Advances in Neural Information Processing Systems*, pp. 271–279, 2016.
- Oh, Junhyuk, Guo, Xiaoxiao, Lee, Honglak, Lewis, Richard L, and Singh, Satinder. Action-conditional video prediction using deep networks in atari games. In *Advances in Neural Information Processing Systems*, pp. 2863–2871, 2015.
- Radford, Alec, Metz, Luke, and Chintala, Soumith. Unsupervised representation learning with deep convolutional generative adversarial networks. *arXiv preprint arXiv:1511.06434*, 2015.
- Saito, Masaki and Matsumoto, Eiichi. Temporal generative adversarial nets. *arXiv preprint arXiv:1611.06624*, 2016.
- Schölkopf, Bernhard and Smola, Alexander J. *Learning with kernels: support vector machines, regularization, optimization, and beyond*. MIT press, 2002.
- Schulman, John, Heess, Nicolas, Weber, Theophane, and Abbeel, Pieter. Gradient estimation using stochastic computation graphs. In *Advances in Neural Information Processing Systems*, pp. 3528–3536, 2015.
- Srivastava, Nitish, Mansimov, Elman, and Salakhudinov, Ruslan. Unsupervised learning of video representations using LSTMs. In *International Conference on Machine Learning*, pp. 843–852, 2015.
- Stuhlmüller, Andreas, Taylor, Jacob, and Goodman, Noah. Learning stochastic inverses. In *Advances in neural information processing systems*, pp. 3048–3056, 2013.
- Tolstikhin, Ilya, Bousquet, Olivier, Gelly, Sylvain, and Schoelkopf, Bernhard. Wasserstein auto-encoders. *arXiv preprint arXiv:1711.01558*, 2017.
- Villegas, Ruben, Yang, Jimei, Hong, Seunghoon, Lin, Xunyu, and Lee, Honglak. Decomposing motion and content for natural video sequence prediction. *arXiv preprint arXiv:1706.08033*, 2017.
- Vondrick, Carl, Pirsivash, Hamed, and Torralba, Antonio. Generating videos with scene dynamics. In *Advances In Neural Information Processing Systems*, pp. 613–621, 2016.
- Warde-Farley, David and Bengio, Yoshua. Improving generative adversarial networks with denoising feature matching. 2016.
- Xue, Tianfan, Wu, Jiajun, Bouman, Katherine, and Freeman, Bill. Visual dynamics: Probabilistic future frame synthesis via cross convolutional networks. In *Advances in Neural Information Processing Systems*, pp. 91–99, 2016.

**Algorithm 3** Inverse factorization

**Input** the associated graph  $\mathcal{G}$  of  $p_{\mathcal{G}}(X, Z)$   
**Output** the inverse factorization  $\mathcal{H}$  of  $q_{\mathcal{H}}(Z|X)$

- Order the latent variables  $Z$  from leaves to roots according to  $\mathcal{G}$
- Initialize  $\mathcal{H}$  as all observable variables  $X$  without any edge

**for**  $z_i \in Z$  **do**

- Add  $z_i$  to  $\mathcal{H}$  and set  $\text{pa}_{\mathcal{H}}(z_i) = \partial_{\mathcal{G}}(z_i) \cap \mathcal{H}$

**end for**

**A. Algorithm for Inverse Factorizations**

We present the formal procedure of building the inverse factorizations in Alg. 3.

**B. The Local Approximation of the JS Divergence**

We now derive the local approximation of the JS divergence.

$$\begin{aligned}
 & \mathcal{D}_{JS}(q(X, Z) || p(X, Z)) \\
 & \approx \mathcal{D}_{JS}(q(A)\overline{q(A)} || p(A)\overline{p(A)}) \\
 & \approx \mathcal{D}_{JS}(q(A)\overline{q(A)} || p(A)\overline{q(A)}) \\
 & = \int q(A)\overline{q(A)} \log \frac{q(A)\overline{q(A)}}{p(A)\overline{q(A)} + q(A)\overline{q(A)}} dX dZ \\
 & \quad + \int p(A)\overline{q(A)} \log \frac{p(A)\overline{q(A)}}{p(A)\overline{q(A)} + q(A)\overline{q(A)}} dX dZ \\
 & = \int q(A)\overline{q(A)} \log \frac{q(A)}{m(A)} dX dZ \\
 & \quad + \int p(A)\overline{q(A)} \log \frac{p(A)}{m(A)} dX dZ \\
 & \approx \int q(A)\overline{q(A)} \log \frac{q(A)}{m(A)} dX dZ \\
 & \quad + \int p(A)\overline{p(A)} \log \frac{p(A)}{m(A)} dX dZ \\
 & \approx \mathbb{E}_q \log \frac{q(A)}{m(A)} + \mathbb{E}_p \log \frac{p(A)}{m(A)},
 \end{aligned}$$

where  $m(A) = \frac{1}{2}(p(A) + q(A))$ . As for the approximations, we adopt two commonly used assumptions: (1)  $q(A) \approx \overline{p(A)}$ , and (2)  $p(X, Z) \approx p(A)p(A)$  and  $q(X, Z) \approx q(A)q(A)$ .

**C. Experimental Details**

In GMGAN, we use the Gumbel-Softmax trick to deal with the discrete variables and the temperature is fixed as 0.1 throughout the experiments. In SSGAN, we use the same  $\epsilon_t$  for all  $t = 1 \dots T$  as the transformation between frames are

Table 2. The generator and extractor on SVHN

Generator $G$	Extractor $E$
Input latent $h$	Input image $x$
MLP 4096 units ReLU Reshape to 4x4x256 5x5 deconv. 128 Stride 2 ReLU 5x5 deconv. 64 Stride 2 ReLU 5x5 deconv. 3 Stride 2 Tanh	5x5 conv. 64 Stride 2 lReLU 5x5 conv. 128 Stride 2 lReLU 5x5 conv. 256 Stride 2 lReLU Reshape to 4096 MLP 128 units Linear
Output image $x$	Output latent $h$

Table 3. The discriminators on SVHN

Global $D_{x,h,k}$	Local $D_{x,h}$ and $D_{h,k}$
Input $(x, h, k)$	Input $(x, h)$ and $(h, k)$
Get $x$ 5x5 conv. 64 Stride 2 lReLU $\alpha$ 0.2 5x5 conv. 128 Stride 2 lReLU $\alpha$ 0.2 5x5 conv. 256 Stride 2 lReLU $\alpha$ 0.2 Reshape to 4096 Concatenate $h$ and $k$ MLP 512 units lReLU $\alpha$ 0.2 Concatenate features of $x$ and $(h, k)$ MLP 512 units lReLU $\alpha$ 0.2 MLP 1 unit Sigmoid	Get $x$ 5x5 conv. 64 Stride 2 lReLU $\alpha$ 0.2 5x5 conv. 128 Stride 2 lReLU $\alpha$ 0.2 5x5 conv. 256 Stride 2 lReLU $\alpha$ 0.2 Reshape to 4096 Get $h$ MLP 512 units lReLU $\alpha$ 0.2 Concatenate features of $x$ and $h$ MLP 512 units lReLU $\alpha$ 0.2 MLP 1 unit Sigmoid
Output a binary unit	Concatenate $h$ and $k$ MLP 512 units lReLU $\alpha$ 0.2 MLP 512 units lReLU $\alpha$ 0.2 MLP 512 units lReLU $\alpha$ 0.2 MLP 1 unit Sigmoid Output two binary units

Table 4. The generator and variant feature extractor on 3D chairs

Generator $G$	Extractor $E_2$
Input latent $(h, v_t)$	Input frame $x_t$
MLP 4096 units ReLU Reshape to 4x4x256 5x5 deconv. 128 Stride 2 ReLU 5x5 deconv. 64 Stride 2 ReLU 5x5 deconv. 32 Stride 2 ReLU 5x5 deconv. 3 Stride 2 Tanh	5x5 conv. 32 Stride 2 lReLU 5x5 conv. 64 Stride 2 lReLU 5x5 conv. 128 Stride 2 lReLU 5x5 conv. 256 Stride 2 lReLU Reshape to 4096 MLP 8 units Linear
Output frame $x_t$	Output latent $v_t$

Table 5. The transition operator and invariant feature extractor on 3D chairs

Generator $O$	Extractor $E_1$
Input latent $v_1$ , noise $\epsilon$	Input video $(x_{1:T})$
Concatenate $v_t$ and $\epsilon$ MLP 256 units lReLU MLP 256 units lReLU MLP 8 units Linear Get $v_t$ MLP 8 units Linear Add the features of $(v_t, \epsilon)$ and $v_t$	Concatenate all frames along channels 5x5 conv. 32 Stride 2 lReLU 5x5 conv. 64 Stride 2 lReLU 5x5 conv. 128 Stride 2 lReLU 5x5 conv. 256 Stride 2 lReLU Reshape to 4096 MLP 128 units Linear
Output $(v_{1:T})$ recurrently	Output latent $h$

Table 6. The discriminators on 3D chairs

ConcatX $D_{x_{1:T}, h, v_{1:T}}$	Local $D_{x_t, h, v_t}$ and $D_{v_t, v_{t+1}}$
Input $(x_{1:T}, h, v_{1:T})$	Input $(x_t, h, v_t)$ and $(v_t, v_{t+1})$
Concatenate all frames along channels $5 \times 5$ conv. 32 Stride 2 IReLU $\alpha$ 0.2 $5 \times 5$ conv. 64 Stride 2 IReLU $\alpha$ 0.2 $5 \times 5$ conv. 128 Stride 2 IReLU $\alpha$ 0.2 $5 \times 5$ conv. 256 Stride 2 IReLU $\alpha$ 0.2 Reshape to 4096 Concatenate $h$ and $v_{1:T}$ MLP 512 units IReLU $\alpha$ 0.2 Concatenate features of $x_{1:T}$ and $(h, v_{1:T})$ MLP 512 units IReLU $\alpha$ 0.2 MLP 1 unit Sigmoid	Get $x_t$ $5 \times 5$ conv. 32 Stride 2 IReLU $\alpha$ 0.2 $5 \times 5$ conv. 64 Stride 2 IReLU $\alpha$ 0.2 $5 \times 5$ conv. 128 Stride 2 IReLU $\alpha$ 0.2 $5 \times 5$ conv. 256 Stride 2 IReLU $\alpha$ 0.2 Reshape to 4096 Concatenate $h$ and $v_t$ MLP 512 units IReLU $\alpha$ 0.2 Concatenate features of $x$ and $h$ MLP 512 units IReLU $\alpha$ 0.2 MLP 1 unit Sigmoid
	Concatenate $v_t$ and $v_{t+1}$ MLP 512 units IReLU $\alpha$ 0.2 MLP 512 units IReLU $\alpha$ 0.2 MLP 512 units IReLU $\alpha$ 0.2 MLP 1 unit Sigmoid
Output a binary unit	Output $2T - 1$ binary units

equivariant on the Moving MNIST and 3D chairs datasets. The batch size varies from 50 to 128, depending on the data.

We present the detailed architectures of Graphical-GAN on the SVHN and 3D chairs datasets in the Tab. 2, Tab. 3, Tab. 4, Tab. 5 and Tab. 6, where  $\alpha$  denotes the ratio of dropout. The architectures on the other datasets are quite similar and please refer to our source code.

## D. More Results of GMGAN

See Fig. 12 and Fig. 13 for the complete results of GMGAN-L on the SVHN, CIFAR10 and CelebA datasets, respectively. We also present the samples of GMGAN-L with 30 clusters on the MNIST dataset in Fig. 14 (a). With larger  $K$ , GMGAN-L can learn intra-class clusters like “2” with loop and “2” without loop, and avoid clustering digits in different classes into the same component. GMGAN-L can also generate meaningful samples given a fixed mixture and linearly distributed latent variables, as shown in Fig. 14 (b) and (c).

## E. More Results of SSGAN

See Fig. 15 for the reconstruction and disentanglement results of SSGAN-L on the Moving MNIST dataset. See for Fig. 16 for the reconstruction results on the 3D chairs datasets.



(a) GMGAN-L ( $K = 50$ ) on the SVHN dataset



(b) GMGAN-L ( $K = 30$ ) on the CIFAR10 dataset

Figure 12. Samples of the GMGAN-L on the SVHN and CIFAR10 datasets. The mixture  $k$  is fixed in each column of (a) and (b).



Figure 13. Samples of GMGAN-L ( $K = 100$ ) on the CelebA dataset.



(a) MNIST ( $K = 30$ )

(b) SVHN ( $K = 50$ )

(c) CelebA ( $K = 100$ )

Figure 14. (a): 30 mixtures of GMGAN-L on the MNIST dataset. (b) and (c): Interpolation results of GMGAN-L on the SVHN and CelebA datasets, respectively. Three endpoints are randomly sampled to construct a parallelogram and other points are linearly distributed.

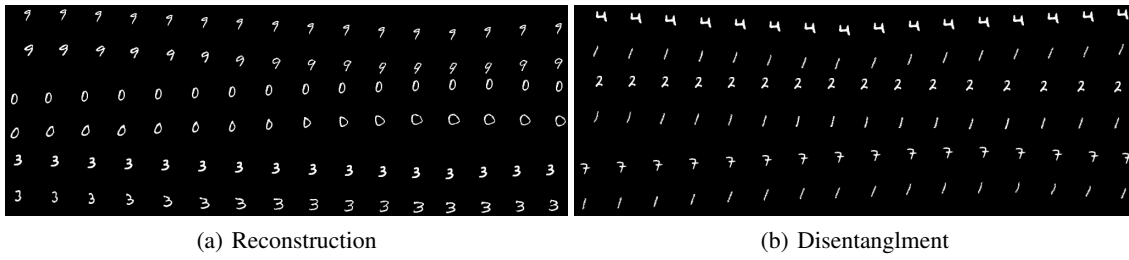


Figure 15. (a) Reconstruction results. Each odd row shows a video in the testing set and the next even row shows the reconstructed video. (b) Disentanglement results. Each odd row shows a video in the testing set and the next even row shows the video generated with a fixed invariant feature  $h$  and the dynamic features  $v$  inferred from the corresponding test video.



Figure 16. Reconstruction results of SSGAN-L on the 3D chairs dataset.